IEEE Access
Multidisciplinary | Rapid Review | Open Access Journal

Received May 26, 2021, accepted June 2, 2021, date of publication June 4, 2021, date of current version June 14, 2021.

Digital Object Identifier 10.1109/ACCESS.2021.3086696

Design and Analysis of Aerial-Terrestrial Network: A Joint Solution for Coverage and Rate

DEEPAK SALUJA[1], ROHIT SINGH[1], (Graduate Student Member, IEEE), KWONHUE CHOI[2], (Senior Member, IEEE), AND SUMAN KUMAR[1]

[1]Department of Electrical Engineering, Indian Institute of Technology Ropar, Rupnagar 140001, India
[2]Department of Information and Communication Engineering, Yeungnam University, Gyeongsan 38541, South Korea

Corresponding author: Kwonhue Choi (gonew@ynu.ac.kr)

This work was supported in part by the Technology Development Program of MSS under Grant S2967489, in part by the National Research Foundation of Korea (NRF) grant funded by the Korean Government (MSIT) under Grant 2021R1A2C1010370, and in part by the 2021 Yeungnam University Research Grant.

ABSTRACT The exploitation of aerial base stations (A-BSs) in conjunction with terrestrial base stations (T-BSs) is envisioned as a promising solution to provide connectivity to devices and user-equipment (UE) in crowded situations (viz. in the sports event) and emergency situations (viz. in the disaster management). However, the use of A-BSs with existing terrestrial networks intensifies the inter-cell interference (ICI) to the devices and UEs, therefore leading to a degraded signal-to-interference-ratio (SIR). This paper addresses this issue by exploiting different radio access technology (RAT) (mmWave/microwave) for aerial and terrestrial networks. Indeed, the network connectivity is always a top priority for all applications. However, there are also some applications such as remote patient monitoring, and remote working, which requires both coverage and high data-rates. But, most of the existing research claims the trade-off between the coverage and the data-rate performance. Whereas this paper aims to improve coverage and rate simultaneously in an aerial-terrestrial networks by employing an optimal combination of mmWave and microwave RAT based on the proposed association strategy. The essential analysis of such an integrated network involves the evaluation of parameters based on the analytic model. Hence, this paper analytically obtains the coverage probability (CP) and average rate expressions for the proposed integrated aerial-terrestrial networks. The analysis is supported by probabilistic models-based simulations that agree closely with analytical results. The results claim that the proposed model leads to improved performance in terms of both CP and average rate. Also, the paper provides parametric analysis for CP and rate with A-BSs height and A-BSs density to enable its practical implementation in 5G/6G technologies.

INDEX TERMS Aerial-terrestrial networks, millimeter-wave RAT, microwave RAT, coverage probability, average rate, stochastic geometry.

I. INTRODUCTION

While the deployment of commercial 5th generation (5G) cellular network is underway in most countries, the research community is talking about the use-cases, requirements and enabling technologies of 6th generation (6G) cellular network [1], [2]. Among their challenges, current 5G cellular networks fall short of handling the connectivity of terrestrial cellular network in the crowded situations (viz. in the sports event) and emergency situations (viz. in the disaster management) due to prominent non-line-of-sight (non-LoS) path and severe shadowing influence via existing terrestrial cellular network [2]. Whereas 6G cellular networks are expected to provide services everywhere and in all situations (i.e., even in crowded and emergency situations) [1], [2]. The research community has recognized the use of aerial networks in conjunction with terrestrial networks (i.e., the aerial-terrestrial networks) as key components to enhance the connectivity in the crowded situations and emergency situations [2]. UAVs can usually be used as aerial networks. In recent years, UAVs have attracted the attention of wireless communications to support terrestrial cellular networks [3]–[5]. It is highly probable that the communication link between aerial base stations (A-BSs) and user equipment (UE) will experience the LoS path. Moreover, the A-BSs could be helpful in load balancing of existing terrestrial cellular network. Although the use of

The associate editor coordinating the review of this manuscript and approving it for publication was Maurizio Magarini.

A-BSs in conjunction with terrestrial base stations (T-BSs) reduces some load on terrestrial cellular networks [6], [7], it intensifies the inter-cell interference (ICI) to the devices and UEs [4]. A visual picture of connectivity and interference impact on reference UE in a typical downlink aerial-terrestrial cellular network is shown in Fig. 1, where we have considered five A-BSs, four T-BSs, and a reference UE. In this figure, both the T-BSs and A-BSs use microwave radio access technology (RAT). Further, Fig. 1 considers that the reference UE (which is terrestrial-UE here) is served by one of the available A-BS, while it experiences interference from all T-BSs and rest of the A-BSs. In other words, microwave-assisted aerial-terrestrial networks lead to a significant reduction in signal-to-interference-ratio (SIR) at the terrestrial UE. Therefore, the challenge is to address the ICI issue, so that the use of A-BS in already existing terrestrial cellular networks does not increase the interference on the terrestrial devices and UEs.

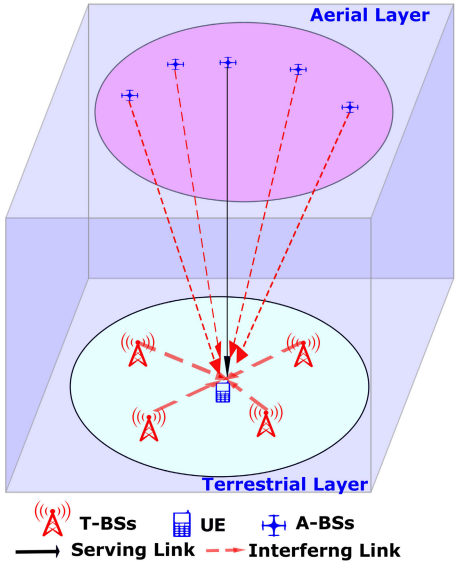

FIGURE 1. Illustration of connectivity and interference in a typical microwave-assisted aerial-terrestrial network.

UAVs have been identified to serve a variety of use cases [6]–[10]. For instance, UAVs as A-BSs could be helpful in load balancing of the existing terrestrial cellular network [6]–[8], especially in crowded situations (e.g., sports event [7], disaster management [6]). They can also be used to temporarily enhance the connectivity at some hotspots [9]. Network connectivity is a key requirement for all these use-cases. Besides, there are also some use cases, including remote patient monitoring [11], [12] and remote working [13], which are more prevalent after the recent COVID-19 pandemic [14]. Even for these use cases, the use of aerial-terrestrial networks is a potential solution to provide connectivity [13]. But these use cases require both good coverage and high data-rate performance in localized areas [13], [15], which cannot be achieved by existing aerial-terrestrial networks.

From the above discussion, we have identified two important challenges. The foremost challenge is that the existing infrastructure which refers to cellular data service via microwave RAT faced strong ICI at microwave RAT. However, similar research has also been conducted at mmWave RAT [8]. But, given the challenges of mmWave RAT in the non-line-of-sight (NLoS) scenario (high path-loss and blockage effects) [8], one cannot rely solely on mmWave RAT for both T-BSs and A-BSs. This paper addresses this challenge of ICI by exploiting different RAT (millimeter-wave (mmWave)/microwave) for aerial and terrestrial networks. Since the mmWave RAT works well under LoS conditions. Therefore, the utilization of mmWave RAT requires its installation at larger heights. So, this paper considers the mmWave RAT for A-BSs and microwave RAT for T-BSs. Whereas, a second challenge that has been identified is to provide good coverage and high data-rate performance for some specified use cases. These requirements of good coverage with high data-rates cannot be achieved by existing aerial-terrestrial networks. Whereas, our work claims the improvement in coverage and the data-rate of the downlink aerial-terrestrial network by employing an optimal combination of mmWave and microwave RAT based on the proposed association strategy. The proposed association strategy is presented in detail in Section II. C. The key differences between the work presented in this paper and the existing works are summarized below.

- The existing works on aerial-terrestrial networks consider either the mmWave RAT or microwave RAT for both the aerial and terrestrial layers. Whereas the work presented in this paper considers an integrated mmWave and microwave framework for aerial-terrestrial networks. This gap between the existing works and presented work ensures that the use of A-BS in existing terrestrial cellular networks does not increase interference on terrestrial devices and UEs.
- The existing research on the aerial-terrestrial networks is progressed in the direction of a trade-off between coverage and data-rate. Whereas the work presented in this paper claims the improvement in both coverage and the data-rate of the downlink aerial-terrestrial networks. This gap between the existing works and presented work ensures the suitability of aerial-terrestrial networks even for the use-cases, including remote patient monitoring and remote working.

A. RELATED WORKS

The investigations of aerial networks have attracted a significant attention by researchers from different perspectives. The 3rd Generation Partnership Project (3GPP) has accepted UAVs suitable for aerial networks [16], [17]. The UAVs as A-BSs are widely discussed in the literature [18]–[20]. Specifically, the authors in [18] provide CP analysis of downlink cellular networks. While the work in [19] considered the A-BSs placement problem to serve the maximum number of terrestrial UEs. An analytical framework for evaluating the CP of cellular-connected aerial networks

is provided in [20]. Note that, in the aforementioned work [18]–[20], A-BSs are assigned microwave RAT. However, the microwave RATs in A-BSs suffer from the challenge of elevated interference. The interference attributes to the dominance of the LoS link between A-BSs and UE. However, the interference mitigation strategies in uplink and downlink scenarios are addressed in [21]. Specifically, the authors considered the power control strategy to reduce interference in the uplink scenario (e.g., by assigning lower power values to UAVs than to terrestrial UEs), while considered a coverage extension strategy to mitigate interference in the downlink scenario. Similarly, the work in [22] addressed the interference mitigation methods in the uplink scenario by formulating an optimization problem based on UAVs uplink cell associations and power allocations. Hence, the microwave RAT assisted A-BSs require the compromise of power level. Besides the interference issues, these microwave-assisted networks may not even meet the high data rate required by some applications.

A solution to the high data-rate demand can be found in mmWave RAT. Recently, the work in [8] provides a comprehensive overview that investigates the feasibility of utilizing mmWave RAT for the aerial networks. The performance of the mmWave assisted aerial network is analyzed in the literature for the condition of heavy traffic in the hot-sport area [9]. It ensures that the mmWave supports a high data rate when utilized at A-BSs. In addition to the performance in terms of high data rate, the mmWave assisted aerial networks are analyzed for coverage performance [23]. Also, the coverage and spectral efficiency analysis for the mmWave-assisted aerial network are presented in [24]. In [6], the authors consider an aerial network for the application to provide coverage to cell-edge UEs in heterogeneous cellular networks. It can be concluded from the discussion that the mmWave promises unprecedented advantages over microwave RAT at A-BSs.

Note that, the more practical scenario is to use A-BSs in conjunction with T-BSs to provide services to UEs. Despite this fact, there is limited work that considers an integrated aerial-terrestrial network [7], [25]–[30]. In particular, the integration of UAVs (aerial networks) with terrestrial networks from the 5G perspective is presented in [25]. While the use of UAV as an A-BSs to help T-BSs by offloading data traffic in crowded areas is presented in [7]. Specifically, the framework in [7] uses microwave RAT for both T-BS and A-BS and aims to maximize the throughput of the downlink single-cell network. However, in our recent work [26], we focused on improving the CP of aerial-terrestrial networks using microwave frequencies in an orthogonal manner. Besides, the work in [27] considered an integrated aerial-terrestrial network where both the T-BS and A-BS share the same microwave spectrum, and analyses downlink and uplink coverage performance. Similar to [27], the authors in [28] investigated the coverage performance of aerial-terrestrial network utilizing microwave RAT. Moreover, the work in [29] considers a downlink aerial-terrestrial network comprising of T-BS and A-BS, where both stations operate at microwave frequency and investigate coverage and rate performance. In [30], the authors analysed the CP and rate of A-UE in an integrated aerial-terrestrial network. These works conclude that the concurrent transmissions from both stations cause interference to each other, consequently degrade the performance of the aerial-terrestrial network.

A stochastic geometry has emerged as a tractable approach to model and analyze the performance of wireless systems via spatial processes, such as the Poisson Point Process (PPP) [23], [31]. Along with ensuring the tractability of mathematical analysis, the PPP assumption assures accuracy in approximating the actual cellular network topology. Most prior work on terrestrial and aerial networks also model the location of T-BSs and A-BSs, respectively, based on PPP [23], [26], [32]–[37]. A similar stochastic geometry analysis via PPP may also be conducted to model the location of T-BSs and A-BSs in aerial-terrestrial networks.

B. OUR CONTRIBUTION

It is evident from the literature that the focus of the existing research on the aerial-terrestrial networks is progressed in the direction of a trade-off between coverage and rate. However, we believe, it is possible to obtain good coverage and rate, considering the optimal combination of mmWave and microwave RAT. To the best of our knowledge, this study have not yet been presented in the literature to date. This paper exploits the merits of mmWave and microwave RAT to improve the performance of downlink aerial-terrestrial network. The aim is to achieve high rate, while maintaining the reliability for the UE. The main contributions of the paper are summarized as follows:

- We model an integrated mmWave and microwave-assisted aerial-terrestrial network. The mmWave RAT is considered for A-BSs, while microwave RAT is considered for T-BSs. In addition, we introduced a novel association strategy for the modeled network that ensures a high data rate along with a good CP of UE. The association strategy is presented in Section II.
- We used the air-to-ground channel model, which considers both LoS and non-LoS (NLoS) transmissions. Using the stochastic geometry framework, an analytical model is developed to analyze the downlink CP and the average rate performance of the modeled network. These analytical results are validated by simulation results.
- We analysed the impact of various parameters (viz. CP and rate) on the network performance, and draw some useful insights into the network design for its practical implementation in 5G/6G technologies. It is shown that differences in CP and average rate between integrated and mmWave networks are significant at a lower density of A-BSs. It means the role of T-BSs is very crucial at a lower density of A-BSs. However, at a higher density of A-BSs, the microwave-assisted T-BSs in the integrated network acts as a backup link to A-BSs.

The summary of main symbols used in the paper are listed in Table 1.

TABLE 1. Summary of main symbols.

Symbol	Description
x_j, y_j, z_o	Location of A-BSs, T-BSs, and the serving BS, respectively
h	Height of A-BSs from the terrestrial layer (ground layer)
$f_{c,m}, f_{c,\mu}$	Carrier frequency of mmWave RAT, microwave RAT, respectively
P_T, P_A	Transmit power of T-BS and A-BS, respectively
S	State of link: LoS (L) or NLoS (N); $S = \{L, N\}$
$\hat{D}_{L,x_j}, \hat{D}_{N,x_j}$	Distance between the typical UE and the LoS A-BS, NLoS A-BS located at point x_j, respectively
D_{y_j}	Distance between the typical UE and the T-BS located at point y_j
$R, \hat{S}_L, \hat{S}_N$	Distance between the typical UE and the nearest T-BS, LoS A-BS, and NLoS A-BS, respectively
$\hat{R}_L, \hat{R}_N$	Distance between the typical UE and the serving BS given that UE is associated to LoS A-BS, and NLoS A-BS, respectively
$\alpha, \hat{\alpha}_L, \hat{\alpha}_N$	Path-loss exponents of a link between typical UE and T-BSs, LoS A-BSs, or NLoS A-BSs, respectively
m_L, m_N	Nakagami-m fading shape parameter for LoS, NLoS aerial link, respectively
σ^2	Thermal noise power
T, S_{th}	Target SIR, SNR threshold
$\lambda_T, \lambda_A, \lambda_L, \lambda_N$	Density of T-BSs, and A-BSs, LoS A-BSs, NLoS A-BSs, respectively
$\psi_T, \psi_A, \psi_{A,L}, \psi_{A,N}$	PPP of T-BSs, and A-BSs, LoS A-BSs, NLoS A-BSs, respectively
g_{y_j}	Channel fading power from typical UE to T-BS located at point y_j
$\hat{g}_{L,x_j}, \hat{g}_{N,x_j}$	Channel fading power from typical UE to LoS A-BS, NLoS A-BS located at point x_j
$p_L(r), p_N(r)$	Probability of LoS, NLoS link between typical UE and A-BS
Υ	SIR experienced by typical UE when it is served by T-BS in proposed aerial-terrestrial network
$\hat{\Lambda}_L, \hat{\Lambda}_N$	SNR experienced by typical UE when it is served by LoS A-BS, NLoS A-BS, respectively in the proposed aerial-terrestrial network

II. SYSTEM MODEL

A. NETWORK MODEL

We consider an aerial-terrestrial network consisting of A-BSs and T-BSs, and focus on the downlink performance. The location of T-BSs are modeled by homogeneous Poisson point process (PPP) on $\mathbb{R}^2$, denoted by $\psi_T \triangleq \{y_i\}$ where y_i refers to the location of i^{th} T-BS, with a density λ_T [TBS/km^2]. While the A-BSs are deployed at a height h, and their location distribution form a another independent homogeneous PPP on $\mathbb{R}^2$, denoted by $\psi_A \triangleq \{x_i\}$ where x_i refers to the location of i^{th} A-BS, with a density λ_A [ABS/km^2]. It is worth mentioning that if A-BS are at different heights (i.e., in 3D space), our framework is still applicable, since the performance of a network of A-BSs with different heights closely matches that of A-BSs deployed at the same height equal to the average of A-BSs heights [29]. Without loss of generality, we assume that a typical UE is located at the origin O of a Cartesian system. Note that all T-BSs and A-BSs transmit at a fixed power of P_T and P_A, respectively.

The A-BSs are assumed to be operated at mmWave RAT, while the T-BSs are assumed to be operated at microwave RAT. The reason for considering mmWave RAT for A-BS is that A-BS often provides LoS channel links with terrestrial UEs, so mmWave RATs can significantly captivate the benefits of such conditions to provide higher data rate. Moreover, the directional antenna array model is considered for mmWave RAT to compensate for the high path-loss and reduce the co-channel interference, which is detailed in the next subsection. While the omnidirectional antenna model is considered for microwave RAT for tractability of analysis. It is notable that our proposed work considers a static A-BS scenario, however, the proposed work can also be extended to a mobile A-BS scenario. In the mobile scenario, the beam alignment between A-BS and UE is challenging, which needs to be updated frequently [38]. Besides, in the literature, different algorithms are proposed to solve the beam alignment issues [39]–[44]. In the mobile scenario, beam alignment algorithms from the literature can be applied first, and then on top of these algorithms, the scheme proposed in this paper can be applied to improve network performance.

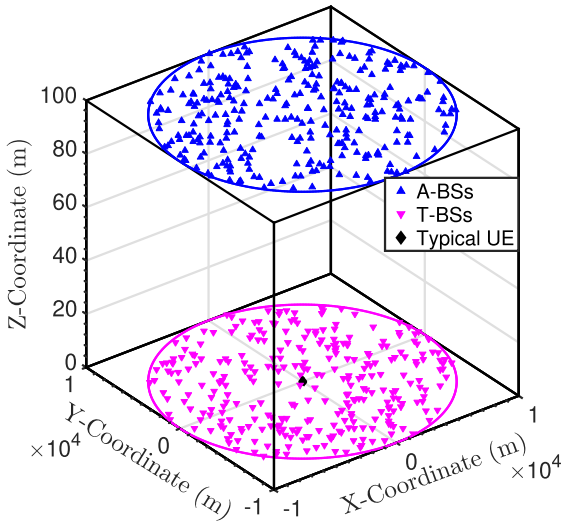

FIGURE 2. Illustration of the network model. The typical UE is located at the origin of Cartesian system. Also, A-BSs and T-BSs are deployed in a circular area according to PPP.

B. CHANNEL MODEL

The transmission of signal via wireless channel is modeled by path-loss attenuation and small-scale fading. However, both the aerial channel and the terrestrial channel have different channel characteristics as follows.

1) AIR-TO-GROUND CHANNEL

According to [7], [9], air-to-ground links are either LoS or NLoS. Their probability of occurrence depends on the buildings height and density, environment, and angle of elevation in between the propagation path of typical UE and UAV. In particular, UAV n is said to be in LoS, if a link connecting typical UE and UAV n does not intersect any obstacles. Here, the LoS probability is modeled as in [7],

$$\hat{p}_L(r) = \frac{1}{1 + C\exp\big[-D(\frac{180}{\pi}sin^{-1}(\frac{h}{r}) - C)\big]}. \quad (1)$$

where C and D are constants that depend on the environment whose value are detailed in Section V, and r is the distance between typical UE and generic A-BS. Similarly, the NLoS probability is given by complementary probability $\hat{p}_N(r) = 1 - \hat{p}_L(r)$. In the air-to-ground channel model, each UE linked

to A-BSs by either a LoS or NLoS transmission. Accordingly, the set of A-BSs ψ_A can be decomposed into two independent PPPs, i.e., $\psi_A = \psi_{A,L} \cup \psi_{A,N}$. Where $\psi_{A,L}$ and $\psi_{A,N}$ denote the set of A-BSs that are in LoS or NLoS state with the reference UE, respectively.

In literature, Rayleigh distribution is the widely used fading model to characterized the NLoS links. While Rician distribution is the appropriate fading model to characterized the LoS links [8]. However, Nakagami-m distribution due to its mathematical tractability is generally used, which can approximate Rician distribution [29]. In particular, Rician fading with Rician factor (K) can be approximated to Nakagami-m fading by setting shape parameter (m) according to its relation with K, given by $m = \frac{(K+1)^2}{2K+1}$. Therefore, this paper assume that LoS aerial links experience Nakagami-m fading with shape parameter m_L and scale parameter $\Omega = \frac{1}{m_L}$, while NLoS aerial links experience Rayleigh fading. However, the Rayleigh fading is the special case of Nakagami-m fading, i.e., Rayleigh fading can be readily obtained from Nakagami-m fading by setting $m = 1$. Therefore, both the LoS and NLoS fading power between typical UE and A-BSs located at point x_j (denoted by $\hat{g}_{S,x_j}$, where $S = \{L, N\}$) can be modeled using a Gamma distribution, that is, $\hat{g}_{S,x_j} \sim \mathcal{G}(m_S, \frac{1}{m_S})$, where its probability density function (pdf) is given by [29],

$$f_{\hat{g}_{S,x_j}}(y) = \frac{m_S{}^{m_S} y^{m_S-1} \exp(-y m_S)}{\Gamma(m_S)}, \tag{2}$$

where $\Gamma(m_S)$ is the Gamma function given by $\Gamma(m_S) = \int_0^\infty z^{m_S-1}\exp(-z)dz$. The path-loss for LoS (L) and NLoS aerial links (N) between the typical UE and the A-BSs located at point x_j is given by: $\hat{L}_S(x_j) = C_S \hat{D}_{S,x_j}^{-\hat{\alpha}_S}$. Here, D_{S,x_j} denote the distances between typical UE and the A-BSs located at point x_j for $S = \{L, N\}$ aerial link transmissions. Also, $\hat{\alpha}_S$ denote the path-loss exponents for the $S = \{L, N\}$ aerial link transmissions. Finally, C_S denote the path-loss gain at unit distance for $S = \{L, N\}$ aerial link transmissions.

Antenna Model: We assume that the A-BSs use directive beamforming to minimize co-channel interference and counterbalance the high path loss [23]. In this work, the antenna array for A-BSs are modeled as a uniform planar array with N_A elements to achieve directive beamforming. It is worth mentioning that for the tractability of the analysis, these antenna patterns can be well approximated by a sectored antenna model [23], [45]. Accordingly, the effective antenna gain of A-BS antenna (denoted by G_A) is modeled as follows:

$$G_A = \begin{cases} G_M, & \text{if } |\psi| \leq \frac{\psi_M}{2}. \\ g_S, & \text{otherwise}, \end{cases} \tag{3}$$

where G_M and g_S denote the main-lobes and side-lobes gains, respectively, ψ denotes the sector angle, and $\psi_M \in [0, \pi]$ denotes the beamwidth in degrees. On the other hand, the interfering links can be modeled as a uniform random variable in $[-\pi, \pi]$ [46]. Hence, the effective antenna gains of the interfering links (denoted by G_I) is G_M with a probability $p_m = \frac{\psi_M}{2\pi}$, and is g_s with a probability $p_s = 1 - \frac{\psi_M}{2\pi}$.

2) TERRESTRIAL CHANNEL

We considered a standard power law path-loss model for terrestrial links. Therefore, the path-loss for terrestrial links between the typical UE and the T-BSs located at point y_j is given by: $L(y_j) = C_0\, D_{y_j}^{-\alpha}$. Here, D_{y_j} denotes the distance between the typical UE and the T-BSs located at point y_j. Also, $C_0 = (\frac{c}{4\pi f_\mu})^2$ defines the path loss gain at unit distance, where c is the velocity of light, and f_μ denotes the operating frequency for microwave RAT. Moreover, α denotes the path-loss exponents of terrestrial link. Besides, we assume that the terrestrial links experience Rayleigh fading, and we consider an omnidirectional antenna model at T-BSs.

C. SINR CALCULATION AND ASSOCIATION STRATEGY

With the use of directional antennas, mmWave networks tend to be noise-limited, rather than the interference-limited, as the beamforming gain obtained by the use of directional antennas significantly minimizes the impact of the co-channel interference [46], [47]. Therefore, without loss of generality, we have considered a noise-limited scenario for the mmWave RAT [46], [47]. Unlike mmWave networks, microwave networks are interference-limited [31]. Therefore, we have considered an interference-limited scenario for the microwave RAT.

The instantaneous SNR (denoted by $\hat{\Lambda}_S$) of proposed integrated aerial-terrestrial network at the typical UE when it connects to either LoS or NLoS A-BS (i.e., $S = \{L, N\}$) located at point $z_0 \in \psi_{A,S}$ is given by

$$\hat{\Lambda}_S = \frac{P_A G_M \hat{g}_{S,z_0} \hat{L}_S(z_0)}{\sigma^2 \mathrm{F}}, \quad \text{if } z_0 \in \psi_{A,S}, \tag{4}$$

where P_A denotes the transmit power of A-BS, $\hat{g}_{S,z_0}$ denotes the LoS or NLoS (i.e., $S = \{L, N\}$) channel fading power from typical UE to serving A-BS located at point z_0, $\hat{L}_S$ is the effective path-loss for aerial links as defined in Section II. B. 1, σ^2 is the thermal noise power modeled as additive white Gaussian noise, and F denotes the noise figure.

The instantaneous SIR (denoted by Υ) of proposed integrated aerial-terrestrial network at the typical UE when it is associated with T-BS located at point $z_0 \in \psi_T$ is given by

$$\Upsilon = \frac{P_T g_{z_0} L(z_0)}{I_{\psi_T/z_0}}, \quad \text{if } z_0 \in \psi_T, \tag{5}$$

where P_T denotes the transmit power of T-BS, g_{z_0} denotes the channel fading power from typical UE to serving T-BS located at point z_0, $L(z_0)$ is the path-loss for terrestrial links as defined in Section II.B.2, and I_{ψ_T/z_o} is the aggregate interference, which comes from set of all T-BSs except the serving T-BS.

$$I_{\psi_T/z_0} = \sum_{y_j \in \psi_T/z_o} P_T g_{y_j} L(y_j). \tag{6}$$

Association Strategy: In the integrated mmWave and microwave networks, each UE may connect to either A-BS (i.e., with mmWave RAT) or T-BS (i.e., with microwave

RAT) based on the association strategy. As discussed earlier, mmWave and microwave RATs have different channel characteristics (i.e., they have different path loss, blockage sensitivity, noise-power, channel bandwidth), which offers a trade-off between the coverage and data-rate performance of mmWave and microwave RATs. For instance, microwave RAT offers good coverage, but data-rate is limited. While mmWave RAT offers good data-rate, but coverage is limited. However, to benefit from both RATs, it is important to use them appropriately. In other words, it is important to consider an appropriate association strategy. The existing highest SNR-based association strategy gives an association preference to the RAT that provides the highest SNR. In the case when the typical user meets the coverage requirements by both mmWave and microwave RAT, the highest SNR-based RAT selection approach does not always take advantage of wideband mmWave RAT to provide enhanced rates. In other words, the SNR-based RAT selection approach may limit the average rate of the system in such a case despite having the capability to increase the data rate. In this paper, we have proposed a threshold based association strategy that improves the average rate of an aerial-terrestrial networks without compromising the coverage probability by employing an optimal combination of mmWave and microwave RAT. As per the proposed association strategy, the association of a typical UE to either T-BS or A-BS is determined based on a predefined threshold (S_{th}). In detail, the association strategy first checks the SNR experienced by a typical UE from the nearest A-BS. If the received SNR is greater than the predefined S_{th}, the typical UE would associate to A-BS. Otherwise, it would associate with T-BS. It means the proposed association strategy gives the association preference to mmWave RAT based on S_{th}. Hence, with this association policy, we can improve the rate of the aerial-terrestrial network. It is worth mentioning that this association strategy also improves the CP of the aerial-terrestrial network. However, to determine the association of typical UE with either LOS A-BS or NLOS A-BS, we considered a highest average received power-based association strategy. In the calculation of highest averaged received power, we set the average small-scale fading power to unity [29]. Based on the highest received power association strategy and the assumption that $\mathbb{E}[\hat{g}_{L,x_j}] = \mathbb{E}[\hat{g}_{N,x_j}] = 1, \forall x_j \in \psi_A$, the serving A-BS is defined as follows:

$$\hat{z}_0 = \arg\max\{C_L \hat{S}_L^{-\hat{\alpha}_L}, C_N \hat{S}_N^{-\hat{\alpha}_N}\}, \tag{7}$$

where $\hat{S}_L = \min_{\forall x_j \in \psi_{A,L}} \hat{D}_{L,x_j}$, and $\hat{S}_N = \min_{\forall x_j \in \psi_{A,N}} \hat{D}_{N,x_j}$.

III. COVERAGE ANALYSIS

The CP of UE is generally defined as the probability that SINR achieved by a randomly chosen UE is greater than a target SINR (T):

$$P_c = \mathbb{P}(\text{SINR} > T). \tag{8}$$

However, the CP computation for the proposed framework includes the following steps. As discussed earlier in previous Section, the reference UE is served by a single BS i.e., by either LoS A-BS, NLoS A-BS, or T-BS. Let E_Q, $Q = \{L, N, T\}$ denotes three disjoint events that the typical UE is associated with a LoS A-BS, NLoS A-BS, or T-BS, respectively. Also, we define the event for the typical UE is in coverage, which is denoted by C. The CP of UE is computed based on the relation: $P_C = \sum_Q \mathbb{P}[C|E_Q]\mathbb{P}[E_Q]$, $Q = \{L, N, T\}$. The CP of UE is computed based on the relation: $P_C = \sum_Q \mathbb{P}[S|E_Q]\mathbb{P}[E_Q]$, $Q = \{L, N, T\}$. Therefore, before proceeding to compute the expressions for the CP, we derive expressions for the probabilities of UEs association with A-BS (using $S = \{L, N\}$ aerial transmission link (denoted by A_S, where $S = \{L, N\}$) or T-BS.

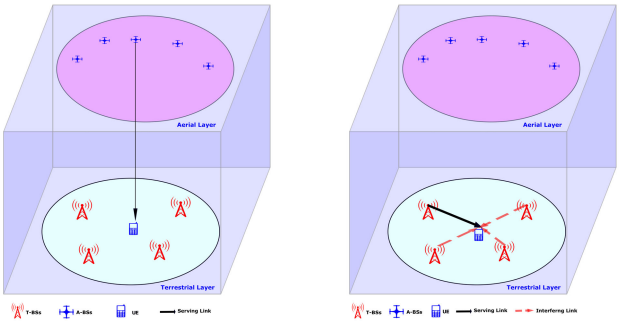

(a) Typical UE is served by A-BS (b) Typical UE is served by T-BS

FIGURE 3. Illustration of connectivity and interference in the proposed integrated mmWave and microwave aerial-terrestrial network. Here, solid black arrows show the desired signal links, while the dotted red arrows show the interfering links.

A. NEAREST INTERFERING BS

From the previous discussion, it can be noticed that interfering T-BSs and A-BSs lie at a distance larger than 0 m, h m, respectively, from the typical UE. However, the clear insight on the distance of nearest interfering BS from the typical UE can be given after knowing the association state of typical UE ($Q = \{L, N, T\}$). The following remark gives clear information on the nearest interfering LoS A-BSs, given that the typical UE is associated to NLoS A-BS. This result is helpful for the computation of main results (i.e., calculation of CP for the proposed network) of this paper.

Remark: Suppose that the typical UE is associated to NLoS A-BS located at a distance r meters, then the nearest interfering LoS A-BS is at least at distance $d_N^L(r)$, which is given by

$$d_N^L(r) = \left(\frac{C_L}{C_N}\right)^{\frac{1}{\alpha_L}} r^{\frac{\alpha_N}{\alpha_L}}. \tag{9}$$

Proof: The average received power of typical UE from the serving NLoS A-BS located at a distance r meters is given by: $P_{r,N} = P_A C_N r^{-\hat{\alpha}_N}$. The nearest interfering LoS A-BS lies at a distance larger than $d_N^L(r)$, which can be computed using the relation $P_A C_N r^{-\hat{\alpha}_N} = P_A C_L d_N^{L\,-\hat{\alpha}_L}(r)$. □

B. DISTANCE DISTRIBUTIONS AND ASSOCIATION PROBABILITIES

To calculate the average association probabilities, CP, and the rate of UE, it is important to obtain the pdf of the distance between the UE and the nearest serving T-BS and A-BS.

Lemma 1: The pdf of the distances between the typical UE and the nearest LoS A-BS, and NLoS A-BS, denoted by $f_{\hat{S}_L}(r)$, *and* $f_{\hat{S}_N}(r)$, *respectively, are given by*

$$f_{\hat{S}_L}(r) = 2\pi\lambda_A r\hat{p}_L(r)exp\Big(-2\pi\lambda_A\int_0^r x\hat{p}_L(x)dx\Big), \quad (10)$$

$$f_{\hat{S}_N}(r) = 2\pi\lambda_A r\hat{p}_N(r)exp\Big(-2\pi\lambda_A\int_0^r x\hat{p}_N(x)dx\Big). \quad (11)$$

Proof: See Appendix A. □

Lemma 2: The pdf of distance between the typical UE and nearest serving T-BS, denoted by $f_R(r)$, *is expressed as*

$$f_R(r) = 2\pi r\lambda_T exp(-\pi\lambda_T r^2), \quad (12)$$

where, $r > 0$.

Proof: The proof for $f_R(r)$ is provided in [31], hence omitted here. □

C. ASSOCIATION PROBABILITIES

As per the association strategy for the proposed integrated network, the typical UE is served by either LoS A-BS, NLoS A-BS, or T-BS. The association probabilities for these three cases are obtained below:

(*i*) Association with NLoS A-BS: The typical UE is associated with NLoS A-BS, if it satisfies the following two conditions. (*a*) the received SNR at the typical UE from the nearest NLoS A-BS is greater than S_{th}, i.e., $\hat{\Lambda}_N > S_{th}$, and (*b*) the power received from the nearest NLoS A-BS is higher than the power received from the nearest LoS A-BS. Combining these two conditions, the probability that the typical UE is served by A-BS via NLoS aerial transmission link is given by

$$A_N = A_N^L A_{m,N}, \quad (13)$$

where $A_{m,N}$ and A_N^L are the mathematical notations, which define the condition (*a*) and condition (*b*), respectively in a probabilistic form. In particular, A_N^L defines the probability that the power received from the nearest NLoS A-BS is higher than the power received from the nearest LoS A-BS. While $A_{m,N}$ defines the probability that the received SNR at the typical UE from the nearest NLoS A-BS is greater than S_{th}. The expression for A_N^L and $A_{m,N}$ are obtained as follows (see lemma 3 and 4).

Lemma 3: The expression for A_N^L *defined in* (13) *is given by*

$$A_N^L = \int_h^\infty exp\Big(-2\pi\lambda_A\int_0^{d_N^L(r)} x\hat{p}_L(x)dx\Big)f_{\hat{S}_N}(r)dr, \quad (14)$$

where $d_N^L(r)$ *is given in* (9), *while* $f_{\hat{S}_N}(r)$ *is given in* (11).

Proof: See Appendix B. □

Lemma 4: The expression for $A_{m,N}$ *defined in* (13) *is given by*

$$A_{m,N} = 1 - \mathbb{E}_{\hat{S}_N}\Big[exp(-\Omega_N n_N)\sum_{k=m_N}^{\infty}\frac{(\Omega_N n_N)^k}{k!}\Big], \quad (15)$$

where $n_N = \frac{S_{th}\sigma^2 F}{P_A G_M \hat{L}_N(z_0)}$.

Proof: See Appendix C. □

(*ii*) Association with LoS A-BS: The typical UE is associated with LoS A-BS, if it satisfies the following two conditions. (*a*) the received SNR at the typical UE from the nearest LoS A-BS is greater than S_{th}, i.e., $\hat{\Lambda}_L > S_{th}$, and (*b*) the power received from the nearest LoS A-BS is higher than the power received from the nearest NLoS A-BS. Combining these two conditions, the probability that the typical UE is served by A-BS via LoS aerial transmission link is given by

$$A_L = A_L^N A_{m,L}, \quad (16)$$

where $A_{m,L}$ and A_L^N are the mathematical notations, which define the condition (*a*) and condition (*b*), respectively in a probabilistic form. In particular, A_L^N defines the probability that the power received from the nearest LoS A-BS is higher than the power received from the nearest NLoS A-BS. While $A_{m,L}$ defines the probability that the received SNR at the typical UE from the nearest LoS A-BS is greater than S_{th}. The expression for A_L^N and $A_{m,L}$ are obtained as follows (see lemma 5).

Lemma 5: The expression for A_L^N *defined in* (16) *is given by*

$$A_L^N = 1 - A_N^L. \quad (17)$$

Proof: The proof of (17) follows from law of total probability, i.e., $A_L^N + A_N^L = 1$. □

Lemma 6: The expression for $A_{m,L}$ *defined in* (13) *is given by*

$$A_{m,L} = 1 - \mathbb{E}_{\hat{S}_L}\Big[exp(-\Omega_L n_L)\sum_{k=m_L}^{\infty}\frac{(\Omega_L n_L)^k}{k!}\Big], \quad (18)$$

where $n_L = \frac{S_{th}\sigma^2 F}{P_A G_M \hat{L}_L(z_0)}$.

Proof: The proof follows the similar process as Lemma 4, so omitted here. □

Remark: The probability that the typical UE is associated with an A-BS is given by $A_{eff} = A_N + A_L$. *This probability defines the average fraction of UEs served by A-BSs.*

(*iii*) *Association with T-BS: The typical UE is served by T-BS, if the received SNR at the typical UE from the nearest A-BS (LoS or NLoS) is less than* S_{th}.

Lemma 7: Given that typical UE is associated to a NLoS A-BS, then pdf of distance between typical UE and serving NLoS A-BS, denoted by $f_{\hat{R}_N}(r)$, *is expressed as follows.*

$$f_{\hat{R}_N}(r) = \frac{f_{\hat{S}_N}(r)}{A_N}exp\Big(-2\pi\lambda_A\int_0^{d_N^L(r)} x\hat{p}_L(x)dx\Big) \times\Big(1 - exp\Big(-2\pi\lambda_A\int_0^{f(S_{th})} x\hat{p}_N(x)dx\Big)\Big). \quad (19)$$

Proof: See Appendix D. □

Lemma 8: Given that typical UE is associated to a LoS A-BS, then pdf of distance between typical UE and serving LoS A-BS, denoted by $f_{\hat{R}_L}(r)$, is expressed as follows.

$$f_{\hat{R}_L}(r) = \frac{f_{\hat{S}_L}(r)}{A_L} exp\Big(- 2\pi\lambda_A \int_0^{d_L^N(r)} x\hat{p}_N(x)dx\Big) \times \Big(1 - exp\Big(- 2\pi\lambda_A \int_0^{f(S_{th})} x\hat{p}_L(x)dx\Big)\Big). \quad (20)$$

Proof: This proof for LoS scenario follows the similar process as Lemma 5, so omitted here. □

D. COVERAGE PROBABILITY CALCULATIONS: MAIN RESULTS

We are now ready to present our main results on CP.

Theorem 9: The average CP contributed by A-BSs in an integrated aerial-terrestrial networks is defined as,

$$\mathcal{P}_{C,A} = \mathcal{P}_{C,A,L}A_L + \mathcal{P}_{C,A,N}A_N, \quad (21)$$

where $P_{C,A,L}$ and $P_{C,A,N}$ define the conditional CP i.e., CP when the typical UE is associated to LoS A-BS and NLoS A-BS, respectively. Also, these expressions for $P_{C,A,L}$ and $P_{C,A,N}$ are given by:

$$\mathcal{P}_{C,A,L} = 1 - \mathbb{E}_{\hat{R}_L}\Big[exp(-\Omega_L x_L)\sum_{k=m_L}^{\infty}\frac{(\Omega_L x_L)^k}{k!}\Big], \quad (22)$$

$$\mathcal{P}_{C,A,N} = 1 - \mathbb{E}_{\hat{R}_N}\Big[exp(-\Omega_N x_N)\sum_{k=m_N}^{\infty}\frac{(\Omega_N x_N)^k}{k!}\Big], \quad (23)$$

where $x_S = \frac{T\sigma^2 F}{P_A G_M \hat{R}_S^{-\hat{\alpha}_S}}$ such that $S = \{L, N\}$.

Proof: See Appendix E. □

The CP contributed by T-BSs in an integrated aerial-terrestrial networks is defined as,

$$\mathcal{P}_{C,T} = \sum_{S\in L,N}\mathbb{P}[\Upsilon_T > T|\hat{\Lambda}_S < S_{th}]\mathbb{P}[\hat{\Lambda}_S < S_{th}]. \quad (24)$$

Theorem 10: The expression for the average CP contributed by T-BSs in an integrated aerial-terrestrial networks is given by,

$$\mathcal{P}_{C,T} = \sum_{S\in L,N}\mathbb{E}_{\hat{S}_S}\Big[exp(-\Omega n)\sum_{k=m}^{\infty}\frac{(\Omega n)^k}{k!}\Big] \times \mathbb{E}_R\Big[exp\{-2\pi\lambda_T G(T,\alpha)\}\Big], \quad (25)$$

where $G(T,\alpha) = \int_r^{\infty}\Big(1 - \frac{1}{1+\frac{TP_T L(u)}{L(z_0)}}\Big)udu$, $\Omega = \frac{1}{m}$, $n = \frac{S_{th}\sigma^2 F}{P_A G_M \hat{L}_S(z_0)}$.

Proof: See Appendix F. □

Theorem 11: The effective CP of proposed integrated mmWave and microwave framework for aerial-terrestrial network is given by

$$\mathcal{P}_{C,Eff} = \mathcal{P}_{C,T} + \mathcal{P}_{C,A}. \quad (26)$$

Proof: The effective CP of proposed integrated mmWave and microwave framework for aerial-terrestrial network can be obtained by adding the resulting expressions of Theorem 10 (which gives the expression for $\mathcal{P}_{C,T}$) and Theorem 9 (which gives the expression for $\mathcal{P}_{C,A}$). □

It is worth mentioning that the closed form expression for the final CP is not feasible, since we do not have a closed form for the integration in (14) and (15) [29]. However, we can still obtain insight of (26) making use of numerical evaluation of the integrals, i.e., CP plot for the proposed network is shown in Section V making use of numerical evaluation of the integrals).

IV. AVERAGE RATE ANALYSIS

In this section, we derive the average rate expressions for the proposed aerial-terrestrial network.

Theorem 12: The average rate of typical UE in the proposed integrated aerial-terrestrial networks is given by,

$$\mathcal{R} = \mathcal{R}_{\mathcal{T}} + \mathcal{R}_L A_L + \mathcal{R}_N A_N, \quad (27)$$

where R_L and R_N define the conditional average rate, i.e., average rate of typical UE given that it is associated to LoS A-BS and NLoS A-BS, respectively. While $\mathcal{R}_T$ defines the average rate contributed by T-BS. The final expressions for $\mathcal{R}_{\mathcal{T}}$, $\mathcal{R}_L$, and $\mathcal{R}_N$ are given by:

$$\mathcal{R}_T = \int_{t>0}\sum_{S\in L,N}\mathbb{E}_{\hat{S}_S}\Big[exp(-\Omega n)\sum_{k=m}^{\infty}\frac{(\Omega n)^k}{k!}\Big] \times \mathbb{E}_R\Big[exp\{-2\pi\lambda_T G(T,\alpha)\}\Big]dt. \quad (28)$$

$$\mathcal{R}_L = 1 - \mathbb{E}_{\hat{R}_L}\Big[\int_{t>0} exp(-\Omega_L x_L)\sum_{k=m_L}^{\infty}\frac{(\Omega_L x_L)^k}{k!}dt\Big], \quad (29)$$

$$\mathcal{R}_N = 1 - \mathbb{E}_{\hat{R}_N}\Big[\int_{t>0} exp(-\Omega_N x_N)\sum_{k=m_N}^{\infty}\frac{(\Omega_N x_N)^k}{k!}dt\Big], \quad (30)$$

where $G(t,\alpha) = \int_r^{\infty}\Big(1 - \frac{1}{1+\frac{(exp(t)-1)P_T L(u)}{L(z_0)}}\Big)udu$, $\Omega = \frac{1}{m}$, $\Omega_L = \frac{1}{m_L}$, $\Omega_N = \frac{1}{m_N}$, $n = \frac{S_{th}\sigma^2 F}{P_A G_M \hat{L}_S(z_0)}$, and $x_S = \frac{exp(t)-1)\sigma^2 F}{P_A G_M \hat{R}_S^{-\hat{\alpha}_S}}$ for $S = \{L, N\}$.

Proof: See Appendix G. □

V. RESULTS AND DISCUSSION

We assume that a typical UE is located at the origin O of a Cartesian system. Also, it is assumed that T-BSs are distributed according to PPP in a 2-D terrestrial layer, while A-BSs are distributed according to another independent PPP in a 2-D aerial layer located at a height of h metres from terrestrial layer. Let the locations of T-BSs and A-BSs are given by $T(x_T, y_T)$ and $A(x_A, y_A, h)$, respectively. Therefore, the distances between typical UE and T-BSs are given by $\sqrt{x_T^2 + y_T^2}$. While the distances between typical UE and A-BSs are given by $\sqrt{x_A^2 + y_A^2 + h^2}$. The simulation

TABLE 2. Simulation parameters [23], [29].

Parameter	Values	
	mmWave RAT	**Microwave RAT**
Fading type	Nakagami-m	Rayleigh
Path gain intercept	$C_L = 10^{-6.14}, C_N = 10^{-7.2}$	$C_0 = (\frac{c}{4\pi f_{c,\mu}})^2$, where $c = 3 \times 10^8$ m/s
Path gain exponent	$\hat{\alpha}_L = 2.09, \hat{\alpha}_N = 3.75$	$\alpha = 3$
Transmit power	20 dBm	40 dBm
Operating frequency	$f_{c,m} = 28$ GHz	$f_{c,\mu} = 2$ GHz
Bandwidth	$B_m = 1$ GHz	$B_\mu = 10$ MHz
BS deployment density	4 A-BSs/km^2	2 T-BSs/km^2
Noise Power	$\sigma^2 = -174$dBm/Hz $+ 10\log_{10} B_m + F$, where F = 10 dB	-
Nakagami-m shape parameter	$m_L = 2; n_N = 1$	1
UAV height	$[50 - 1000]$ m	
Target SIR/SNR	$[-10 : 10]$ dB	
SNR threshold	$S_{th} = [-5, 0]$ dB	

parameters with their values used to plot the results are listed in Table 2.

For typical UE, we generate an exponential fading power for the nearest serving T-BS and a gamma fading power for the nearest serving A-BS. Moreover, we generate an exponential fading power corresponding to its terrestrial interferers and a gamma fading power corresponding to its aerial interferers. Then, we compute the SIR of the terrestrial layer and SNR of the aerial layer. The CP contributed by A-BSs and T-BSs for the proposed network is then evaluated, which are averaged over 10^5 iterations. The CP contributed by A-BSs is calculated based on the following two conditions: (*i*) the received SNR at UEs from the nearest A-BS must be greater than S_{th}, that is, $\Lambda_A > S_{th}$; and (*ii*) the received SNR of mmWave UEs must be greater than T, that is, $\Lambda_A > T$. While the CP contributed by T-BSs is calculated based on the following two conditions: (*i*) the received SNR at UEs from the nearest A-BS must be less than S_{th}; and (*ii*) the received SIR from associated microwave T-BS is greater than T, that is, $\Upsilon_T > T$. The average rate ($\mathcal{R}$) of the proposed network is evaluated according to the Shannon formula, that is, using the relation, $\mathcal{R} = \mathbb{E}[\ln(1 + \text{SINR})]$, which are averaged over 10^5 iterations.

A. COVERAGE ANALYSIS

Fig. 4 compares the CP of proposed networks with conventional mmWave networks[1] and conventional microwave networks.[2] It can be observed from Fig. 4 that the proposed networks has higher CP than conventional mmWave networks and microwave networks. The reason for the higher CP compared to the conventional mmWave network is that the use of microwave RAT in the proposed network can compensate for the effects of high path loss and blockage effect at the mmWave frequency. Whereas the reason for the higher CP than the microwave network is that the proposed network uses the mmWave RAT for A-BSs and microwave RAT for T-BSs, hence eliminates the dominant LoS interference from A-BSs to UEs. Moreover, it can be seen that the analytical results closely match with the simulation results.

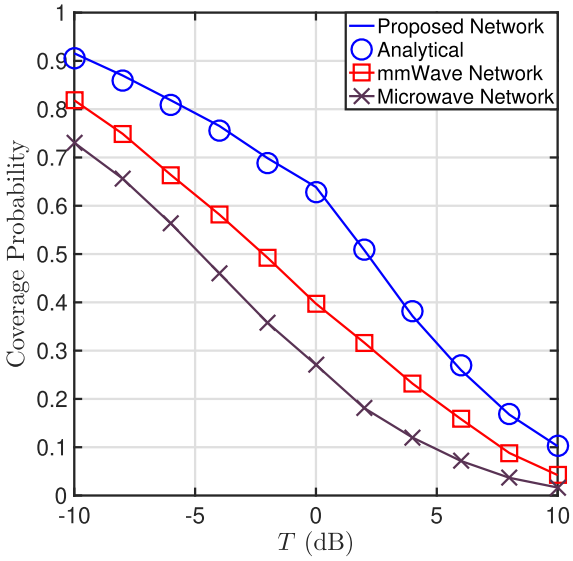

FIGURE 4. CP comparison of proposed network with conventional mmWave and microwave network. Here, $S_{th} = 0$ dB, and $h = 100$ m.

The individual CP contributed by T-BSs and A-BSs in the proposed network is shown in Fig. 5. Note that, $S_{th} = 0$ dB is taken to compute the CP. As discussed earlier, the CP contributed by A-BSs is calculated as $\mathbb{P}[\Lambda_A > \max(T, S_{th})]$. Therefore, for the considered scenario with $S_{th} = 0$ dB and $T < 0$ dB, the CP contributed by A-BSs can be simplified as $\mathbb{P}[\Lambda_A > S_{th}]$, which is independent of T. Therefore, the CP contributed by A-BSs is constant till $T = 0$ dB. While for $T > 0$ dB, the CP contributed by A-BSs can be simplified as $\mathbb{P}[\Lambda_A > T]$. Therefore, the CP decreases with the increase in T after $T > 0$. On the other hand, the CP contributed by T-BSs decreases with an increase in T.

B. RATE ANALYSIS

Fig. 6 shows the average rate variation of the typical UE with the density of A-BSs (ABS/km^2) for mmWave network,

[1] conventional mmWave network is the one that considers mmWave RAT for both T-BSs and A-BSs.

[2] conventional microwave network is the one that considers microwave RAT for both T-BSs and A-BSs [29].

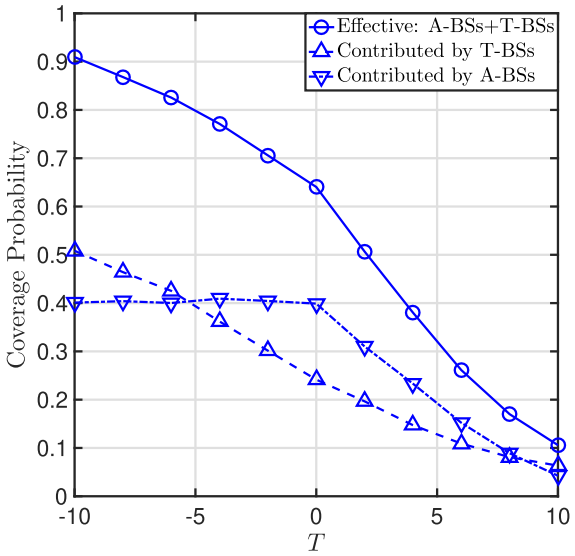

FIGURE 5. CP contributed by mmWave-assisted A-BSs and microwave-assisted T-BSs in the proposed network. Here, $S_{th} = 0$ dB, $G_m = 20$ dB, and $h = 100$ m.

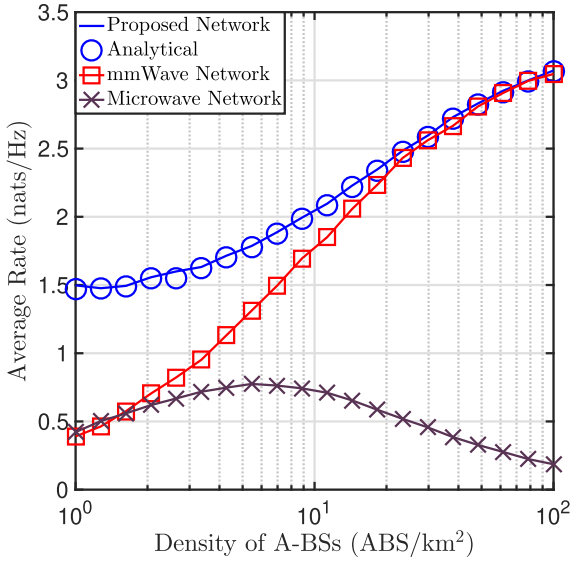

FIGURE 6. Average rate variation of the typical UE with density of A-BSs (ABS/km^2) for mmWave network, microwave network, and proposed network. Here, $S_{th} = 0$ dB, $G_m = 20$ dB, and $h = 100$ m.

microwave network, and proposed network. The following observations can be made from the plots:

- The proposed network has a higher average rate than the both microwave-assisted aerial-terrestrial network and the mmWave-assisted aerial-terrestrial network. The reason is that the association strategy for the proposed network gives the association preference to A-BSs (that are assigned a mmWave RAT) based on the value of S_{th}, which ensures higher data rates without compromising CP. However, at higher A-BS densities, the average rate for the proposed network approaches the average rate for the mmWave network.

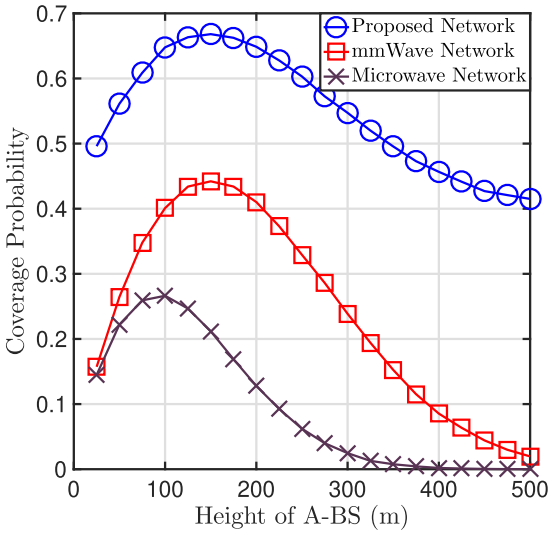

FIGURE 7. CP versus height of A-BS for mmWave network, microwave network, and proposed network. Here, $S_{th} = 0$ dB, $G_m = 20$ dB, $h = 100$ m.

TABLE 3. LoS probability parameters [29].

Environment	Parameters	
	C	Y
Suburban	4.88	0.43
Urban	9.6117	0.1581
Dense Urban	11.95	0.136
High-rise Urban	27.23	0.08

- The average rate for the proposed network and mmWave network increase with A-BS density. This is because as the density of A-BS increases, the probability that a typical UE is associated with an LoS A-BS increases. Thus, the probability that a typical UE is associated with an interference dominated T-BS decreases. This combination of association probability with T-BS and A-BS effectively improves the signal power while reduces the interference power, and therefore the average rate increases with A-BS density.

C. IMPACT OF A-BS HEIGHT

Fig. 7 shows the variation of CP with the height of A-BS for mmWave network, microwave network, and proposed network. It can be observed from Fig. 7, the plots of CP for all networks exhibit the similar trend, i.e., the CP initially increases with the height of A-BS and then decreases. Note that, for each network, there is a height at which the CP is maximum. For the proposed network and mmWave assisted aerial-terrestrial network, the probability that the UEs experience LoS condition with A-BSs initially increases with the increase in A-BS height while the path-loss due to mmWave RAT is less dominating than the gain provided by LoS links. Hence, in this region, the CP increases with the height of A-BS. However, with a further increase in A-BS height, the CP decreases, even though UE may be served by LoS A-BS. This is due to the fact that as the

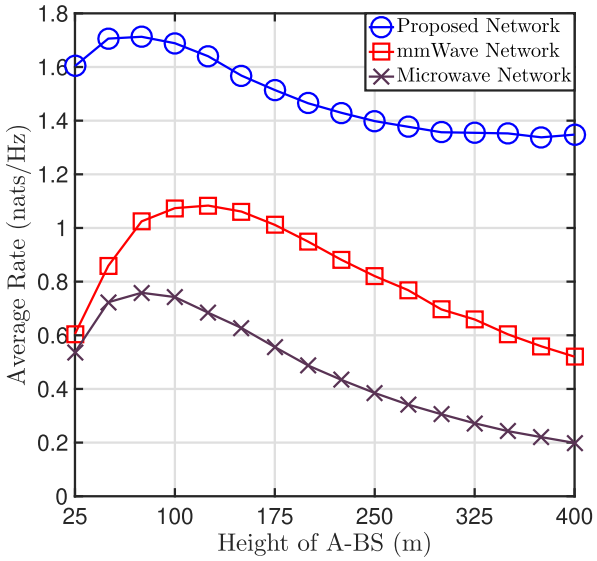

FIGURE 8. Average rate variation with respect to height of A-BS for mmWave, microwave, and proposed network. Here, $S_{th} = 0$ dB, and $G_m = 20$ dB.

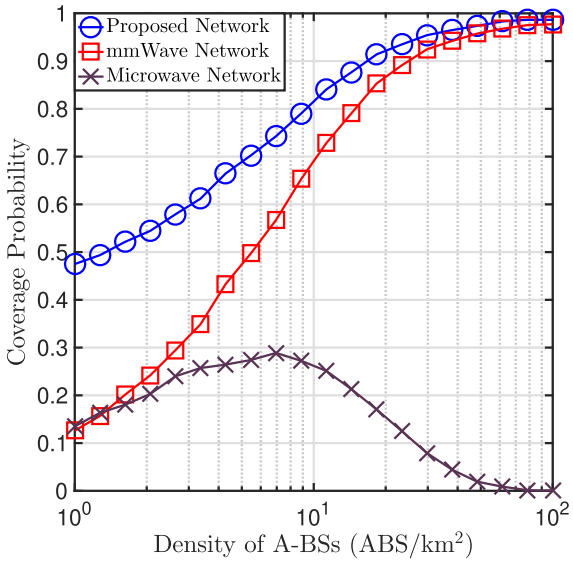

FIGURE 9. CP versus A-BSs density for mmWave network, microwave network, and proposed network. Here, $S_{th} = 0$ dB, $G_m = 20$ dB, and $h = 100$ m.

height of A-BS increases beyond a certain value, signal power decreases owing to increase in path-loss with A-BS height. Likewise, for microwave-assisted aerial-terrestrial network, the probability for a UE to experience LoS condition with A-BSs initially increases with the increase in A-BS height. As a result, both signal power and interference power from A-BSs decreases. However, the signal power dominates the interference power up to a certain A-BS height, beyond this value the interference power begins to dominate the signal power. Hence, the CP initially increases with the height of A-BS and then decreases.

Fig. 8 shows the variation of average rate with respect to the height of A-BS for mmWave network, microwave network, and proposed network. As can be seen from Fig. 8, the different curves for all the networks exhibit the same trend, i.e., the CP initially increases with the height of A-BS and then decreases. The reason for this is similar to the CP plots in Fig. 7.

D. IMPACT OF BS DENSITY

Fig. 9 plots the CP with respect to A-BS density for the mmWave network, microwave network, and proposed network. It can be observed that CP for the proposed network increases with A-BS density. This is because as the density of A-BS increases, the probability that a typical UE is associated with an LoS A-BS increases. As a result, the probability of typical UE associating with an interference dominated T-BS decreases. This combination of association probability with T-BS and A-BS effectively improves the signal power while reduces the interference power, and therefore the CP of proposed network increases with A-BS density. The individual CP contributed by T-BSs and A-BSs in the proposed network is shown in Fig. 10. As expected, the CP contribution by

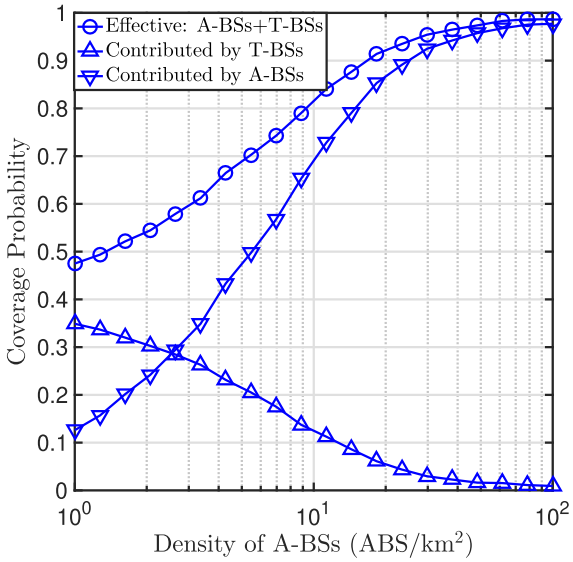

FIGURE 10. Plot shows the CP contributed by A-BSs, T-BSs, and A-BSs + T-BSs in the proposed network with the A-BSs density (ABS/km^2). Here, $S_{th} = 0$ dB, $G_m = 20$ dB, and $h = 100$ m.

A-BSs increase with the increase of A-BSs density. Thus, the load on T-BSs decreases.

E. IMPACT OF ENVIRONMENT

To analyze the impact of environment on the performance of proposed system, the values for LoS probability parameters under different environment are listed in Table 3. In Fig. 11, we compare the CP of proposed network for different environments. As expected, the CP decreases as the surroundings becomes denser (i.e., as the height and density of building increases). The reason is that for dense scenario, the probability for typical user to experience a NLoS conditions with

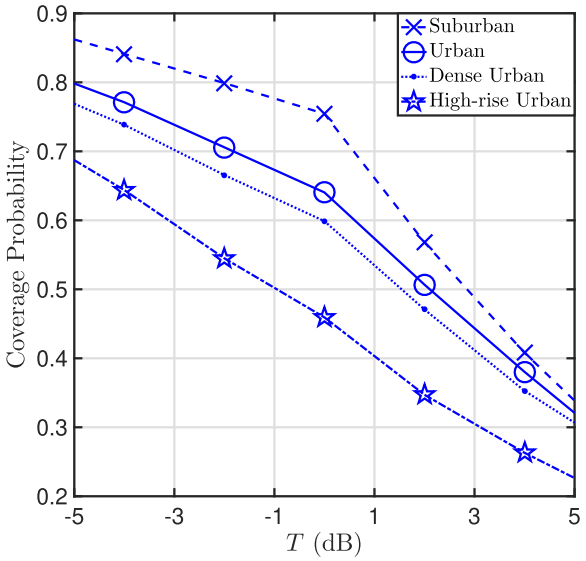

FIGURE 11. CP versus T for different aerial channel environments. Here, $S_{th} = 0$ dB, $G_m = 20$ dB, and $h = 100$ m.

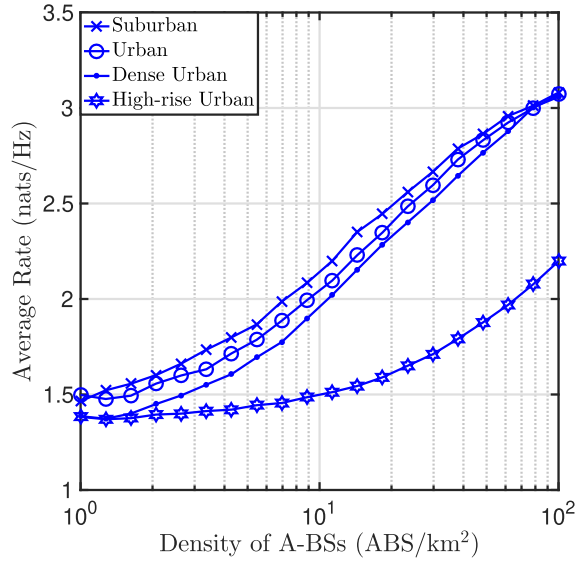

FIGURE 12. Average rate versus density of A-BSs (ABS/km^2) for different aerial channel environments. Here, $S_{th} = 0$ dB, $G_m = 20$ dB, and $h = 100$ m.

A-BSs decreases. Hence the received power from serving A-BSs decreases. Consequently, the role of interference dominated T-BSs becomes more prominent. Hence, the effective CP decreases as the surroundings becomes denser. Fig. 12 compare the average rate of proposed network for different environments. The comparison presents the same observations, as presented by CP comparisons for different environments, i.e., average rate decreases as the surroundings becomes denser.

VI. CONCLUSION

In this work, we consider the downlink aerial-terrestrial network, where both the mmWave and microwave interfaces are used together. The performance of such a network is analyzed in terms of CP, and average rate. Further, the performance of the proposed network is compared with mmWave network. The results claim that the proposed model leads to improved performance in terms of both CP and average rate. Also, the paper provides parametric analysis for CP and rate with A-BSs height and A-BSs density to enable its practical implementation in 5G/6G technologies. It is shown that differences in CP and average rate between integrated and mmWave networks are significant at a lower density of A-BSs. It means that the role of T-BSs is very crucial at a lower density of A-BSs. However, at a higher density of A-BSs, the microwave-assisted T-BSs in the integrated network acts as a backup link to A-BSs.

It is noteworthy that our proposed work provides analysis for static A-BS scenarios. However, the work proposed under the static A-BS scenario can be extended to the mobile A-BS scenario. In addition, beam alignment between BS and UE is a challenging problem in mobile networks, allowing the present work to be extended to include beam alignment issue in the future work.

APPENDIX A
PROOF OF LEMMA 1

Consider a LoS scenario, where the typical UE communicates with the nearest LoS A-BS separated by a distance r. Since all UEs communicate with the nearest LoS A-BSs, no other LoS A-BSs lie nearer than the distance r. The cdf of the distance between the typical UE and the nearest LoS A-BS is given by

$$\begin{aligned} F_{\hat{S}_L}(r) &= 1 - \mathbb{P}[\text{No LoS A-BS nearer than } r] \\ &= 1 - \mathbb{P}[\hat{S}_L > r] \\ &\overset{(a)}{=} 1 - \exp\Big(- 2\pi \int_0^r x\lambda_L(x)dx \Big) \\ &\overset{(b)}{=} 1 - \exp\Big(- 2\pi\lambda_A \int_0^r x\hat{p}_L(x)dx \Big). \end{aligned} \tag{31}$$

Here (a) follows from the void probability of PPP, while (b) follows from the fact that $\lambda_L(x) = \lambda_A \hat{p}_L(x)$. Finally, the pdf of $\hat{S}_L(r)$ is computed using the relation: $f_{\hat{S}_L} = \frac{d}{dr} F_{\hat{S}_L}(r)$. The resulting expression proves the lemma for LoS scenario. With the same steps as for calculating $f_{\hat{S}_L}$, one can also prove the lemma for $f_{\hat{S}_N}$ (i.e., for NLoS scenario).

APPENDIX B
PROOF OF LEMMA 3

Let A_N^L denotes the probability that the power received from the nearest NLoS A-BS is higher than the power received from the nearest LoS A-BS. Hence, the probability that the typical UE is associated to A-BS via NLoS aerial transmission link is given by

$$\begin{aligned} A_N^L &= \mathbb{P}\big[P_A C_N \hat{S}_N^{-\alpha_N} > P_A C_L \hat{S}_L^{-\alpha_L}\big] \\ &= \mathbb{P}\left[\hat{S}_L > \left(\frac{C_L}{C_N}\right)^{\frac{1}{\alpha_L}} \hat{S}_N^{\frac{\alpha_N}{\alpha_L}}\right] \\ &\overset{(a)}{=} \mathbb{P}\big[\hat{S}_L > d_N^L(\hat{S}_N)\big] \end{aligned}$$

$$\stackrel{(b)}{=} \int_h^{\infty} \mathbb{P}\big[\hat{S}_L > d_N^L(r)\big] f_{\hat{S}_N}(r) dr. \tag{32}$$

Here the step (a) in (32) follows from (9). While the step (b) is to conditioned the resultant expression over the nearest NLoS A-BS (i.e., average over pdf $f_{\hat{S}_N}$). Finally, use the void probability of PPP to complete the proof of A_N^L.

APPENDIX C
PROOF OF LEMMA 4

$A_{m,N}$ defines the probability that the received SNR at the typical UE from the nearest NLoS A-BS is greater than S_{th}.

$$A_{m,N} = \mathbb{P}[\hat{\Lambda}_N > S_{th}] = \mathbb{P}\left[\frac{P_A G_M \hat{g}_{N,z_0} \hat{L}_N(z_0)}{\sigma^2 \mathrm{F}} > S_{th}\right]$$
$$= \mathbb{E}_{\hat{S}_N}\left[\mathbb{P}\left(\hat{g}_{N,z_0} > \frac{S_{th}\sigma^2 \mathrm{F}}{P_A G_M \hat{L}_N(z_0)}\right)\right]. \tag{33}$$

Since $\hat{g}_{N,z_0} \sim \mathcal{G}(m_N, \Omega_N = \frac{1}{m_N})$, we can further solve Eq. (33) by deriving the cumulative distribution function (CDF) of the random variable $X_N = g_{N,z_0}$, as below:

$$F_{X_N}(x_N; m_N, \Omega_N) = \mathbb{P}[g_{N,z_0} \le x_N]$$
$$= \frac{\gamma(m_N, \Omega_N x_N)}{\Gamma(m_N)}; \ x_N \ge 0, \ m_N \ge 0, \tag{34}$$

where $\gamma(m_N, \Omega_N x_N)$ is the lower incomplete gamma function, given by, $\gamma(m_N, \Omega_N x_N) = \int_0^{\Omega_N x_N} t^{m_N - 1}\exp(-t)dt$, and $\Gamma(m_N)$ is the gamma function, given by $\Gamma(m_N) = \int_0^{\infty} t^{m_N-1}\exp(-t)dt = (m_N - 1)!$. Therefore, (33) becomes

$$= 1 - \mathbb{E}_{\hat{S}_N}\left[\frac{\int_0^{\Omega_N x_N} t^{m_N-1}\exp(-t)dt}{(m_N - 1)!}\right]. \tag{35}$$

For $m > 0$, (35) can also be expressed by the series expansion as given in (33). This completes the proof of lemma.

APPENDIX D
PROOF OF LEMMA 7

The pdf of $\hat{R}_N(r)$ is computed from the pdf of $\hat{S}_N(r)$, i.e., the pdf of $\hat{R}_N(r)$ is the pdf of $\hat{S}_N$ given that the typical UE is associated with a NLoS A-BS (i.e., given that event E_N has occurred). It can be written as

$$f_{\hat{R}_N}(r) = \frac{d}{dr}\mathbb{P}(\hat{R}_N(r) \le r) = \frac{d}{dr}\mathbb{P}(\hat{S}_N(r) \le r | E_N)$$
$$= \frac{d}{dr}\frac{\mathbb{P}(\hat{S}_N(r) \le r, E_N)}{\mathbb{P}(E_N)}. \tag{36}$$

Using (32), the numerator in (36) can be expressed as follows:

$$\mathbb{P}(\hat{S}_N(r) \le r, E_N)$$
$$\stackrel{(a)}{=} \mathbb{P}\big(\{\hat{S}_N(r) \le r\} \cap \{\hat{S}_L(r) > d_N^L(r) \cap \hat{S}_N(r) < f(S_{th})\}\big)$$
$$= \mathbb{P}\big(\{\hat{S}_N(r) \le r \cap \hat{S}_L(r) > d_N^L(r)\} \cap$$
$$\times \{\hat{S}_N(r) \le r \cap \hat{S}_N(r) < f(S_{th})\}\big)$$
$$\stackrel{(b)}{=} \int_h^r \mathbb{P}(\hat{S}_L(r) > d_N^L(r))\mathbb{P}(\hat{S}_N(r) < f(S_{th})) f_{\hat{S}_N(r)} dr. \tag{37}$$

Here the step (a) in (37) is follows from (32), where $f(S_{th}) = \left(\frac{S_{th}\sigma^2 F}{P_A G_M C_N}\right)^{-\frac{1}{\hat{\alpha}_L}}$. Note that the lower limit of integration in step (b) is h, because the nearest NLoS A-BS from the typical UE is at atleast a distance h. Now using the void probability of PPP, we get

$$\mathbb{P}(\hat{S}_N(r) \le r, E_N)$$
$$= \int_h^r \exp\Big(-2\pi\lambda_A \int_0^{d_N^L(r)} x\hat{p}_L(x)dx\Big)$$
$$\times \Big(1 - \exp\Big(-2\pi\lambda_A \int_0^{f(S_{th})} x\hat{p}_N(x)dx\Big)\Big) f_{\hat{S}_N(r)} dr. \tag{38}$$

Finally, substituting (38) into (36), and then differentiating the resulting expression gives (19), which completes the proof of lemma.

APPENDIX E
PROOF OF THEOREM 9

Given that the typical UE is associated with a LoS A-BS, the conditional CP $P_{C,A,L}$ is given by

$$\mathcal{P}_{C,A,L} = \mathbb{P}[\hat{\Lambda}_L > T]$$
$$= \mathbb{E}_{\hat{R}_L}\left[\mathbb{P}\left(\hat{g}_{L,z_0} > \frac{T\sigma^2 \mathrm{F}}{P_A G_M C_L \hat{R}_L^{-\hat{\alpha}_L}}\right)\right]. \tag{39}$$

Since $\hat{g}_{L,z_0} \sim \mathcal{G}(m_L, \Omega = \frac{1}{m_L})$, we can further solve Eq. (39) by deriving the cumulative distribution function (CDF) of the random variable $X = g_{L,z_0}$, as below:

$$F_X(x; m, \Omega) = \mathbb{P}[g_{L,z_0} \le x]$$
$$= \frac{\gamma(m_L, \Omega_L x_L)}{\Gamma(m_L)}; \ x_L \ge 0, \ m_L \ge 0, \tag{40}$$

where $\gamma(m_L, \Omega_L x_L)$ is the lower incomplete gamma function, given by, $\gamma(m_L, \Omega_L x_L) = \int_0^{\Omega_L x_L} t^{m_L-1}\exp(-t)dt$, and $\Gamma(m_L)$ is the gamma function, given by $\Gamma(m_L) = \int_0^{\infty} t^{m_L-1}\exp(-t)dt = (m_L - 1)!$. Therefore, $\mathcal{P}_{C,A,L}$ in (39) becomes

$$\mathcal{P}_{C,A,L} = 1 - \mathbb{E}_{\hat{R}_L}\left[\frac{\int_0^{\Omega_L x_L} t^{m_L-1}\exp(-t)dt}{(m_L - 1)!}\right]. \tag{41}$$

Here, $x_L = \frac{T\sigma^2 \mathrm{F}}{P_A G_M \hat{R}_L^{-\hat{\alpha}_L}}$. For $m > 0$, (41) can be expressed by the following series expansion,

$$\mathcal{P}_{C,A,L} = 1 - \mathbb{E}_{\hat{R}_L}\left[\exp(-\Omega_L x_L)\sum_{k=m_L}^{\infty}\frac{(\Omega_L x_L)^k}{k!}\right]. \tag{42}$$

This completes the proof of Theorem 1. The proof of the conditional CP $P_{C,A,N}$ follows a similar method as that of $P_{C,A,L}$, therefore omitted here.

APPENDIX F
PROOF OF THEOREM 10

The CP contributed by T-BSs in an integrated aerial-terrestrial network is defined as

$$\mathcal{P}_{C,T} = \mathbb{P}[\Upsilon > T | \hat{\Lambda}_S < S_{th}]\mathbb{P}[\hat{\Lambda}_S < S_{th}]. \tag{43}$$

Upon applying Bayes' rule, (43) can be rewritten as

$$\mathcal{P}_{C,T} = \mathbb{P}[\Upsilon > T, \hat{\Lambda}_S < S_{th}] = \mathbb{P}\Big[\frac{P_T g_{z_0} L(z_0)}{I_{\psi_T/z_0}} > T, \frac{P_A G_M \hat{g}_{S,z_0} \hat{L}_S(z_0)}{\sigma^2 \mathrm{F}} < S_{th}\Big]. \quad (44)$$

Since both g_{z_0} and $\hat{g}_{S,z_0}$ are assumed to be independent, $\mathcal{P}_{c,T}$ can be simplified as

$$\mathcal{P}_{C,T} = \mathbb{P}\Big[\frac{P_T g_{z_0} L(z_0)}{I_{\psi_T/z_0}} > T\Big] \times \mathbb{P}\Big[\frac{P_A G_M \hat{g}_{S,z_0} \hat{L}_S(z_0)}{\sigma^2 \mathrm{F}} < S_{th}\Big]. \quad (45)$$

Here, the second term in (45) can be solved as follows:

$$\mathbb{P}\Big[\frac{P_A G_M \hat{g}_{S,z_0} \hat{L}_S(z_0)}{\sigma^2 \mathrm{F}} < S_{th}\Big] = 1 - \mathbb{E}_{\hat{S}_S}\Big[\mathbb{P}\Big(\hat{g}_{S,z_0} > \frac{S_{th}\sigma^2 \mathrm{F}}{P_A G_M \hat{L}_S(z_0)}\Big)\Big]. \quad (46)$$

Here $\hat{S}_S = \{\hat{S}_L, \hat{S}_N\}$ define the distances from typical UE to nearest LoS A-BS ($\hat{S}_L$) and NLoS A-BS ($\hat{S}_N$). Eq. (46) can be further solved by following the same steps as in (39)-(42). Therefore, the final simplified expression is given as

$$\mathbb{P}\Big[\frac{P_A G_M \hat{g}_{S,z_0} \hat{L}_S(z_0)}{\sigma^2 \mathrm{F}} < S_{th}\Big] = \mathbb{E}_{\hat{S}_S}\Big[\exp(-\Omega_S n_S) \sum_{k=m_S}^{\infty} \frac{(\Omega_S n_S)^k}{k!}\Big], \quad (47)$$

where $n_S = \frac{S_{th}\sigma^2 \mathrm{F}}{P_A G_M \hat{L}_S(z_0)}$. While the first term in (45) can be solved as follows:

$$\mathbb{P}\Big[\frac{P_T g_{z_0} L(z_0)}{I_{\psi_T/z_0}} > T\Big] = \mathbb{E}_R\Big[\mathbb{P}\Big(g_{z_0} > \frac{T I_{\psi_T/z_0}}{P_T L(z_0)}\Big)\Big]. \quad (48)$$

Here $\mathbb{E}_R(.)$ denotes the expectation over the distance form the typical UE to nearest T-BS. Since $g_{z_0} \sim \exp(1)$, (48) can be expressed as

$$\mathbb{P}\Big[g_{z_0} > \frac{T I_{\psi_T/z_0}}{P_T L(z_0)}\Big] = \mathbb{E}_R\Big[\mathbb{E}_{I_{\psi_T/z_0}}\Big[\exp\Big(-\frac{T I_{\psi_T/z_0}}{P_T L(z_0)}\Big)\Big]\Big] = \mathbb{E}_R\Big[\mathcal{L}_{I_{\psi_T/z_0}}\Big(\frac{T}{P_T L(z_0)}\Big)\Big], \quad (49)$$

where $\mathcal{L}_{I_{\psi_T/z_0}}(s)$ denotes the Laplace transform of random variable $I_{\psi_T/z_0}(s)$ evaluated at s. According to the Laplace transform definition

$$\mathcal{L}_{I_{\psi_T/z_0}}(s) = \mathbb{E}_{I_{\psi_T/z_0}}\big[\exp(-sI_{\psi_T/z_0})\big] = \mathbb{E}_{\psi_T/z_0, g_{T,y_j}}\Big[\exp\Big(-s\sum_{y_j \in \psi_T/z_o} P_T g_{y_j} L(y_j)\Big)\Big] = \mathbb{E}_{\psi_T/z_0}\Big[\prod_{y_j \in \psi_T/z_o} \mathbb{E}_{g_{y_j}}\Big[\exp\Big(-sP_T g_{y_j} L(y_j)\Big)\Big]\Big]. \quad (50)$$

Using the fact that random variable g_{y_j} follows an exponential distribution with unit mean, i.e., $g_{y_j} \sim \exp(1)$, (50) can be written as

$$\mathcal{L}_{I_{\psi_T/z_0}}(s) = \mathbb{E}_{\psi_T/z_0}\Big[\prod_{y_j \in \psi_T/z_o} \frac{1}{1 + sP_T L(y_j)}\Big] = \exp\Big\{-2\pi\lambda_T \int_r^{\infty} \Big(1 - \frac{1}{1 + sP_T L(u)}\Big) u du\Big\}. \quad (51)$$

Note that the lower limit of the integral in (51) is r due to the fact that all the interfering T-BSs are at least a distance greater than r. Substituting $s = \frac{T}{P_T L(z_0)}$ in (51), we get

$$\mathcal{L}_{I_{\psi_T/z_0}}\Big(\frac{T}{P_T L(z_0)}\Big) = \exp\Big\{-2\pi\lambda_T \int_r^{\infty} \Big(1 - \frac{1}{1 + \frac{TP_T L(u)}{L(z_0)}}\Big) u du\Big\} = \exp\{-2\pi\lambda_T G(T, \alpha)\}, \quad (52)$$

where $G(T, \alpha) = \int_r^{\infty} \Big(1 - \frac{1}{1 + \frac{TP_T L(u)}{L(z_0)}}\Big) u du$. Substitute the final expression of (52) in (49), we get the resultant expression for the first term of (45). Then, multiply the obtained expression with (47) to obtain the resultant expression for $\mathcal{P}_{c,T}$, given by (25). This completes the proof of Theorem 8.

APPENDIX G
PROOF OF THEOREM 12

The average rate is generally defined as $\mathcal{R} = \mathbb{E}[\ln(1 + \Upsilon)]$ (nats/Hz). For any positive random variable X, $\mathbb{E}[X] = \int_{t>0} \mathbb{P}(X > t) dt$. Therefore, the average rate contributed by T-BSs in proposed aerial-terrestrial network can be expressed as

$$\mathcal{R}_T = \int_{t>0} \mathbb{P}[\ln(1 + \Upsilon) > t] dt = \int_{t>0} \mathbb{P}[\Upsilon > \exp(t) - 1] dt. \quad (53)$$

Using (53) and definition of CP, $\mathcal{R}_T$ can be obtained from (25) by substituting $T = \exp(t) - 1$, and then integrating the resultant expression over t. This completes the proof of Theorem 10 for T-BSs. The prrof for $\mathcal{L}, \mathcal{N}$ follows the same steps as that of $\mathcal{R}_T$, so omitted here.

REFERENCES

[1] S. Dang, O. Amin, B. Shihada, and M.-S. Alouini, "What should 6G be?" *Nature Electron.*, vol. 3, no. 1, pp. 20–29, Jan. 2020.
[2] M. Giordani and M. Zorzi, "Non-terrestrial networks in the 6G era: Challenges and opportunities," *IEEE Netw.*, vol. 35, no. 2, pp. 244–251, Mar. 2021.
[3] B. Li, Z. Fei, and Y. Zhang, "UAV communications for 5G and beyond: Recent advances and future trends," *IEEE Internet Things J.*, vol. 6, no. 2, pp. 2241–2263, Apr. 2019.
[4] M. Mozaffari, W. Saad, M. Bennis, Y.-H. Nam, and M. Debbah, "A tutorial on UAVs for wireless networks: Applications, challenges, and open problems," *IEEE Commun. Surveys Tuts.*, vol. 21, no. 3, pp. 2334–2360, 3rd Quart., 2019.
[5] H. Wang, H. Zhao, W. Wu, J. Xiong, D. Ma, and J. Wei, "Deployment algorithms of flying base stations: 5G and beyond with UAVs," *IEEE Internet Things J.*, vol. 6, no. 6, pp. 10009–10027, Dec. 2019.

[6] H. Wu, Z. Wei, Y. Hou, N. Zhang, and X. Tao, "Cell-edge user offloading via flying UAV in non-uniform heterogeneous cellular networks," *IEEE Trans. Wireless Commun.*, vol. 19, no. 4, pp. 2411–2426, Apr. 2020.

[7] J. Lyu, Y. Zeng, and R. Zhang, "UAV-aided offloading for cellular hotspot," *IEEE Trans. Wireless Commun.*, vol. 17, no. 6, pp. 3988–4001, Jun. 2018.

[8] L. Zhang, H. Zhao, S. Hou, Z. Zhao, H. Xu, X. Wu, Q. Wu, and R. Zhang, "A survey on 5G millimeter wave communications for UAV-assisted wireless networks," *IEEE Access*, vol. 7, pp. 117460–117504, 2019.

[9] F. Zhou, W. Li, L. Meng, and M. Kadoch, "Capacity enhancement for hotspot area in 5G cellular networks using mmWave aerial base station," *IEEE Wireless Commun. Lett.*, vol. 8, no. 3, pp. 677–680, Jun. 2019.

[10] H. Shakhatreh, A. H. Sawalmeh, A. Al-Fuqaha, Z. Dou, E. Almaita, I. Khalil, N. S. Othman, A. Khreishah, and M. Guizani, "Unmanned aerial vehicles (UAVs): A survey on civil applications and key research challenges," *IEEE Access*, vol. 7, pp. 48572–48634, 2019.

[11] V. Oleshchuk and R. Fensli, "Remote patient monitoring within a future 5G infrastructure," *Wireless Pers. Commun.*, vol. 57, no. 3, pp. 431–439, Apr. 2011.

[12] H. Ullah, N. G. Nair, A. Moore, C. Nugent, P. Muschamp, and M. Cuevas, "5G communication: An overview of vehicle-to-everything, drones, and healthcare use-cases," *IEEE Access*, vol. 7, pp. 37251–37268, 2019.

[13] N. Saeed, A. Bader, T. Y. Al-Naffouri, and M.-S. Alouini, "When wireless communication faces COVID-19: Combating the pandemic and saving the economy," 2020, *arXiv:2005.06637*. [Online]. Available: http://arxiv.org/abs/2005.06637

[14] V. Chamola, V. Hassija, V. Gupta, and M. Guizani, "A comprehensive review of the COVID-19 pandemic and the role of IoT, drones, AI, blockchain, and 5G in managing its impact," *IEEE Access*, vol. 8, pp. 90225–90265, 2020.

[15] Y. Ren, R. Werner, N. Pazzi, and A. Boukerche, "Monitoring patients via a secure and mobile healthcare system," *IEEE Wireless Commun.*, vol. 17, no. 1, pp. 59–65, Feb. 2010.

[16] *Study on Enhanced LTE Support for Aerial Vehicles*, document TR 22.125, V17.1.0, 3GPP, 2017.

[17] *Unmanned Aerial System (UAS) Support in 3GPP*, document TR 22.125, V17.1.0, 3GPP, 2019.

[18] M. M. Azari, F. Rosas, A. Chiumento, and S. Pollin, "Coexistence of terrestrial and aerial users in cellular networks," in *Proc. IEEE Globecom Workshops (GC Wkshps)*, Dec. 2017, pp. 1–6.

[19] M. Alzenad, A. El-Keyi, and H. Yanikomeroglu, "3-D placement of an unmanned aerial vehicle base station for maximum coverage of users with different QoS requirements," *IEEE Wireless Commun. Lett.*, vol. 7, no. 1, pp. 38–41, Feb. 2018.

[20] X. Yu, J. Zhang, R. Schober, and K. B. Letaief, "A tractable framework for coverage analysis of cellular-connected UAV networks," in *Proc. IEEE Int. Conf. Commun. Workshops (ICC Workshops)*, May 2019, pp. 1–6.

[21] V. Yajnanarayana, Y.-P. E. Wang, S. Gao, S. Muruganathan, and X. Lin Ericsson, "Interference mitigation methods for unmanned aerial vehicles served by cellular networks," in *Proc. IEEE 5G World Forum (5GWF)*, Jul. 2018, pp. 118–122.

[22] W. Mei, Q. Wu, and R. Zhang, "Cellular-connected UAV: Uplink association, power control and interference coordination," *IEEE Trans. Wireless Commun.*, vol. 18, no. 11, pp. 5380–5393, Nov. 2019.

[23] M. Boschiero, M. Giordani, M. Polese, and M. Zorzi, "Coverage analysis of UAVs in millimeter wave networks: A stochastic geometry approach," in *Proc. Int. Wireless Commun. Mobile Comput. (IWCMC)*, Jun. 2020, pp. 351–357.

[24] W. Yi, Y. Liu, Y. Deng, and A. Nallanathan, "Clustered UAV networks with millimeter wave communications: A stochastic geometry view," *IEEE Trans. Commun.*, vol. 68, no. 7, pp. 4342–4357, Jul. 2020.

[25] I. Bor-Yaliniz, M. Salem, G. Senerath, and H. Yanikomeroglu, "Is 5G ready for drones: A look into contemporary and prospective wireless networks from a standardization perspective," *IEEE Wireless Commun.*, vol. 26, no. 1, pp. 18–27, Feb. 2019.

[26] D. Saluja and S. Kumar, "Modelling and performance analysis of FFR-aided two layer aerial-terrestrial network," *IET Commun.*, vol. 14, no. 5, pp. 736–745, Mar. 2020.

[27] X. Zhou, S. Durrani, J. Guo, and H. Yanikomeroglu, "Underlay drone cell for temporary events: Impact of drone height and aerial channel environments," *IEEE Internet Things J.*, vol. 6, no. 2, pp. 1704–1718, Apr. 2019.

[28] M. G. Khoshkholgh, K. Navaie, H. Yanikomeroglu, V. C. M. Leung, and K. G. Shin, "Coverage performance of aerial-terrestrial HetNets," in *Proc. IEEE 89th Veh. Technol. Conf. (VTC-Spring)*, Apr. 2019, pp. 1–5.

[29] M. Alzenad and H. Yanikomeroglu, "Coverage and rate analysis for vertical heterogeneous networks (VHetNets)," *IEEE Trans. Wireless Commun.*, vol. 18, no. 12, pp. 5643–5657, Dec. 2019.

[30] N. Cherif, M. Alzenad, H. Yanikomeroglu, and A. Yongacoglu, "Downlink coverage and rate analysis of an aerial user in integrated aerial and terrestrial networks," 2019, *arXiv:1905.11934*. [Online]. Available: http://arxiv.org/abs/1905.11934

[31] J. G. Andrews, F. Baccelli, and R. K. Ganti, "A tractable approach to coverage and rate in cellular networks," *IEEE Trans. Commun.*, vol. 59, no. 11, pp. 3122–3134, Nov. 2011.

[32] B. Galkin, J. Kibilda, and L. A. DaSilva, "A stochastic model for UAV networks positioned above demand hotspots in urban environments," *IEEE Trans. Veh. Technol.*, vol. 68, no. 7, pp. 6985–6996, Jul. 2019.

[33] C. Fan, T. Zhang, and Z. Zeng, "Coverage and rate analysis of cache-enabled vertical heterogeneous networks," *IEEE Access*, vol. 7, pp. 153519–153532, 2019.

[34] Y. Qin, M. A. Kishk, and M.-S. Alouini, "Performance evaluation of UAV-enabled cellular networks with battery-limited drones," *IEEE Commun. Lett.*, vol. 24, no. 12, pp. 2664–2668, Dec. 2020.

[35] E. Turgut and M. C. Gursoy, "Downlink analysis in unmanned aerial vehicle (UAV) assisted cellular networks with clustered users," *IEEE Access*, vol. 6, pp. 36313–36324, 2018.

[36] D. Kim, J. Lee, and T. Q. S. Quek, "Multi-layer unmanned aerial vehicle networks: Modeling and performance analysis," *IEEE Trans. Wireless Commun.*, vol. 19, no. 1, pp. 325–339, Jan. 2020.

[37] X. Wang and M. C. Gursoy, "Coverage analysis for energy-harvesting UAV-assisted mmWave cellular networks," *IEEE J. Sel. Areas Commun.*, vol. 37, no. 12, pp. 2832–2850, Dec. 2019.

[38] M. Hashemi, A. Sabharwal, C. E. Koksal, and N. B. Shroff, "Efficient beam alignment in millimeter wave systems using contextual bandits," in *Proc. IEEE Conf. Comput. Commun. (IEEE INFOCOM)*, Apr. 2018, pp. 2393–2401.

[39] I. Chafaa, E. V. Belmega, and M. Debbah, "One-bit feedback exponential learning for beam alignment in mobile mmWave," *IEEE Access*, vol. 8, pp. 194575–194589, 2020.

[40] W. Ma, C. Qi, and G. Y. Li, "Machine learning for beam alignment in millimeter wave massive MIMO," *IEEE Wireless Commun. Lett.*, vol. 9, no. 6, pp. 875–878, Jun. 2020.

[41] M. T. Dabiri, H. Safi, S. Parsaeefard, and W. Saad, "Analytical channel models for millimeter wave UAV networks under hovering fluctuations," *IEEE Trans. Wireless Commun.*, vol. 19, no. 4, pp. 2868–2883, Apr. 2020.

[42] J. Zhang, Y. Huang, Y. Zhou, and X. You, "Beam alignment and tracking for millimeter wave communications via bandit learning," *IEEE Trans. Commun.*, vol. 68, no. 9, pp. 5519–5533, Sep. 2020.

[43] W. Zhang, W. Zhang, and J. Wu, "UAV beam alignment for highly mobile millimeter wave communications," *IEEE Trans. Veh. Technol.*, vol. 69, no. 8, pp. 8577–8585, Aug. 2020.

[44] Y.-N.-R. Li, B. Gao, X. Zhang, and K. Huang, "Beam management in millimeter-wave communications for 5G and beyond," *IEEE Access*, vol. 8, pp. 13282–13293, 2020.

[45] W. Yi, Y. Liu, E. Bodanese, A. Nallanathan, and G. K. Karagiannidis, "A unified spatial framework for UAV-aided mmWave networks," *IEEE Trans. Commun.*, vol. 67, no. 12, pp. 8801–8817, Dec. 2019.

[46] M. Di Renzo, "Stochastic geometry modeling and analysis of multi-tier millimeter wave cellular networks," *IEEE Trans. Wireless Commun.*, vol. 14, no. 9, pp. 5038–5057, Sep. 2015.

[47] S. Singh, M. N. Kulkarni, A. Ghosh, and J. G. Andrews, "Tractable model for rate in self-backhauled millimeter wave cellular networks," *IEEE J. Sel. Areas Commun.*, vol. 33, no. 10, pp. 2196–2211, Oct. 2015.

DEEPAK SALUJA received the B.Tech. degree in electronics and communication engineering from Kurukshetra University, India, in 2013, and the M.Tech. degree in wireless communication from Thapar University, India, in 2015. He is currently pursuing the Ph.D. degree in electrical engineering with IIT Ropar, India. His research interests include radio resource allocation, RF interference management, UAV communication, vehicular communication, and the IoT connectivity.

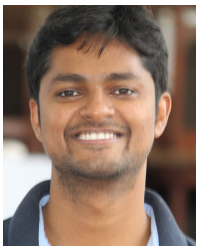

ROHIT SINGH (Graduate Student Member, IEEE) received the B.Tech. degree from the Moradabad Institute of Technology, Moradabad, India, in 2014, and the M.Tech. degree from NIT Jalandhar, India, in 2017. He is currently pursuing the Ph.D. degree with the Department of Electrical Engineering, IIT Ropar, India. His research interests include self-driving vehicles, vehicular communication, and the IoT connectivity.

KWONHUE CHOI (Senior Member, IEEE) received the B.S., M.S., and Ph.D. degrees in electronic and electrical engineering from the Pohang University of Science and Technology, Pohang, South Korea, in 1994, 1996, and 2000, respectively. From 2000 to 2003, he was with the Electronics and Telecommunications Research Institute, Daejeon, South Korea, as a Senior Research Staff Member. In 2003, he joined the Department of Information and Communication Engineering, Yeungnam University, Gyeongsan, South Korea, where he is currently a Professor. He has authored a textbook: *Problem-Based Learning in Communication Systems Using MATLAB and Simulink* (Wiley, 2016). His research interests include signal design for the communication systems, multiple access schemes, diversity schemes for wireless fading channels, multiple antenna systems, and in-band full duplex systems.

SUMAN KUMAR received the B.Tech. degree in electronics and communication engineering from the Future Institute of Engineering and Management, Kolkata, India, in 2010, and the Ph.D. degree from IIT Madras, in 2016. He is currently an Assistant Professor with IIT Ropar. His research interests include performance analysis of wireless networks, including RF interference management, HetNets, vehicular communication, and the IoT networks.